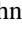










Probabilistic Reconstruction of Type Ia Supernova SN 2002bo

John T. O'Brien¹ , Wolfgang E. Kerzendorf^{1,2} , Andrew Fullard¹, Marc Williamson³ , Rüdiger Pakmor⁴ , Johannes Buchner⁵ , Stephan Hachinger⁶, Christian Vogl^{4,7}, James H. Gillanders⁸ , Andreas Flörs⁹, and Patrick van der Smagt^{10,11} 

¹Department of Physics and Astronomy, Michigan State University, East Lansing, MI 48824, USA; jobrien585@gmail.com, obrie278@msu.edu

²Department of Computational Mathematics, Science, and Engineering, Michigan State University, East Lansing, MI 48824, USA

³Department of Physics, New York University, New York, NY, 10003, USA

⁴Max-Planck-Institut für Astrophysik, Karl-Schwarzschild-Str. 1, D-85748 Garching, Germany

⁵Max-Planck-Institut für extraterrestrische Physik, Giessenbachstrasse 1, D-85748 Garching bei München, Germany

⁶Leibniz Supercomputing Centre, Boltzmannstr. 1, D-85748 Garching bei München, Germany

⁷Exzellenzcluster ORIGINS, Boltzmannstr. 2, D-85748 Garching, Germany

⁸Astrophysics Research Centre, School of Mathematics and Physics, Queen's University Belfast, BT7 1NN, UK

⁹GSI Helmholtzzentrum für Schwerionenforschung, Planckstraße 1, D-64291 Darmstadt, Germany

¹⁰Machine Learning Research Lab, Volkswagen AG, Munich, Germany

¹¹Faculty of Informatics, Eötvös Loránd University, Budapest, Hungary

Received 2021 April 22; revised 2021 June 22; accepted 2021 July 5; published 2021 July 29

Abstract

Manual fits to spectral time series of Type Ia supernovae have provided a method of reconstructing the explosion from a parametric model but due to lack of information about model uncertainties or parameter degeneracies direct comparison between theory and observation is difficult. In order to mitigate this important problem we present a new way to probabilistically reconstruct the outer ejecta of the normal Type Ia supernova SN 2002bo. A single epoch spectrum, taken 10 days before maximum light, is fit by a 13-parameter model describing the elemental composition of the ejecta and the explosion physics (density, temperature, velocity, and explosion epoch). Model evaluation is performed through the application of a novel rapid spectral synthesis technique in which the radiative transfer code, TARDIS, is accelerated by a machine-learning framework. Analysis of the posterior distribution reveals a complex and degenerate parameter space and allows direct comparison to various hydrodynamic models. Our analysis favors detonation over deflagration scenarios and we find that our technique offers a novel way to compare simulation to observation.

Unified Astronomy Thesaurus concepts: [Supernovae \(1668\)](#); [Type Ia supernovae \(1728\)](#); [Bayesian statistics \(1900\)](#); [Radiative transfer \(1335\)](#)

1. Introduction

Type Ia supernovae (SNe Ia) are a spectral class of supernovae defined by their lack of hydrogen lines and the presence of silicon lines. SNe Ia are caused by the thermonuclear explosion of carbon–oxygen white dwarfs in binary systems forming a large amount of ⁵⁶Ni, which drives the behavior of their light curves (Colgate & McKee 1969). They contribute significantly to the chemical evolution of their host galaxies through the dispersion of iron-peak elements formed during the explosion (Kobayashi et al. 2020, see their Figure 39).

Their ability to act as standardizable candles (Phillips 1993) has served as a powerful tool in constraining cosmological parameters (Branch 1992; Riess et al. 1998), though there remains significant variation in their brightness that is unaccounted for (e.g., Blondin et al. 2012). Furthermore, the identification of the ignition mechanism leading to SNe Ia remains an area of active research (see e.g., Polin et al. 2019).

The community has identified multiple promising pathways to explosions, many of which originate in a binary system. For example, nuclear burning may be ignited by either the merger of two CO white dwarfs (e.g., Nomoto 1982; Webbink 1984; Iben & Tutukov 1984; van Kerkwijk et al. 2010; Livio & Riess 2003; Kashi & Soker 2011), or accretion from a companion star-forming a near-Chandrasekhar-mass CO white dwarf causing a central ignition (e.g., Whelan & Iben 1973), or accretion of a helium layer onto a sub-Chandrasekhar-mass white dwarf (e.g., Woosley & Weaver 1994; Fink et al. 2010a; Shen et al. 2018; Polin et al. 2019)

leading to a surface helium detonation that propagates inward triggering central ignition.

Various models have been proposed to describe the processes underlying SNe Ia. In particular, the speed at which the nuclear burning propagates through the star remains poorly understood. Reconstructing the explosion from spectral time series (also known as abundance tomography) is a crucial tool to understand the explosion scenario (see e.g., Mazzali et al. 2007). Previous work into abundance tomography (e.g., Stehle et al. 2005; Sauer & Mazzali 2008) has begun to show us a picture of how SN Ia explosions compare to theoretical models, but they lack a probabilistic interpretation of their parameters.

SN 2002bo is a “Branch normal” (Branch et al. 1993; Benetti et al. 2004; Branch et al. 2006) SN Ia discovered in NGC 3190 that has been modeled extensively in the literature (e.g., Stehle et al. 2005; Sauer & Mazzali 2008; Benetti et al. 2004; Kerzendorf 2011). Specifically, Stehle et al. (2005) used a multi-line Monte-Carlo code to manually reconstruct the explosion mechanism using 13 epochs of spectra. Their inference suggests an SNe Ia with moderate amounts of mixing of ⁵⁶Ni and intermediate-mass elements, as well as a lack of carbon in the ejecta, indicating a possible explosion asymmetry and orientation effects.

While these results offer a good foray into the investigation of the abundance tomography of SNe Ia, the lack of uncertainty or error analysis limits our ability to constrain the range of possible explosion scenarios. Physical sources of uncertainty

Table 1
The Range of Parameters Sampled from Our Prior Distribution along with Their Estimates Determined by the Posterior Distribution

Parameter	Prior Bounds		Posterior Percentiles		
	Minimum	Maximum	16%	50%	84%
C	2.3×10^{-6}	0.17	9.5×10^{-5}	0.0015	0.0085
Mg	8.3×10^{-6}	0.036	0.00011	0.00049	0.0047
Si	0.029	0.58	0.17	0.21	0.26
S	0.005	0.19	0.074	0.09	0.11
Ca	0.00043	0.039	0.0021	0.0034	0.0084
Ti	4.4×10^{-7}	3.7×10^{-5}	2.7×10^{-6}	4.7×10^{-6}	9.7×10^{-6}
Cr	3.8×10^{-5}	0.0022	0.00021	0.00034	0.00062
Fe _{stable}	0.0011	0.1	0.044	0.052	0.065
⁵⁶ Ni	0.037	0.85	0.078	0.091	0.13
T_{inner} (K)	8000	18000	10383	10720	11357
v_{inner} (km s ⁻¹)	7000	20000	13100	13508	14291
α_{ρ}	-10	-6	-6.10	-6.36	-6.63
t_{exp} (days)	6	13	6.32	6.64	7.21
$\log_{10} s$	-18	-14	-15.91	-15.81	-15.69

Note. The abundance distributions are based upon log-uniform sampling but modifications are made in order to assure that the sum of abundance parameters add to unity. All other values displayed are sampled uniformly. For a full description of the abundance sampling method, see Section 3.1. Elemental abundances are shown in terms of mass fractions. Estimates from the posterior distribution are presented as the median with the edges of the 68% confidence interval.

such as line-blending, as well as potential parameter degeneracies, warrant the need for probability distributions.

In this work, we present a method of Bayesian inference of supernova parameters by applying the radiative transfer code TARDIS, accelerated by a machine-learning framework (Kerzendorf et al. 2021), to a single spectrum of SN 2002bo taken 10 days before maximum light (Benetti et al. 2004). We begin with a description of our model and associated parameters in Section 2. The sampling of the parameter space, including a discussion on prior distributions and resulting posterior distributions, is given in Section 3. A summary of results can be found in Section 4. Appendices are included to provide general background on the techniques used for spectral synthesis acceleration as well as additional data used in our analysis. In Appendix A, we outline a machine-learning framework used to accelerate TARDIS evaluation. Finally, in Appendix B, links to data sources and data products are provided in order to assist researchers who wish to replicate our findings.

2. Explosion Model

The optical spectrum of SN 2002bo 10 days before maximum light is modeled with spectral synthesis produced by the radiative transfer code TARDIS. TARDIS is a modular framework that allows for the use of various physics modules and has been widely used for modeling a range of photospheric SNe (e.g., Magee et al. 2016; Barna et al. 2017; Boyle et al. 2017; Gillanders et al. 2020; Vogl et al. 2020; Williamson et al. 2021). TARDIS approximates the radiation field in the ejecta with an optically thick inner boundary and an optically thin homologously expanding ejecta above. There is no energy generation in the simulation area and the energy injection is purely set by the temperature, T_{inner} , and radius, r_{inner} , of this inner boundary. The optically thin ejecta is divided into a series of concentric shells in velocity space. The velocity of each shell is determined by the inner boundary velocity, v_{inner} , and increases linearly up to an outer velocity boundary. The radius of the inner boundary, r_{inner} , and consequently the radius of the

shells, are set by the product of v_{inner} with the time since the explosion, t_{exp} .

We employ a power-law relationship of the density with the velocity parameterized by the power-law index α_{ρ} such that $\rho_{\text{shell}} \propto v_{\text{shell}}^{\alpha_{\rho}}$.¹² In previous works (Stehle et al. 2005; Kerzendorf 2011), the density profile of SN Ia ejecta has been described by a one-dimensional parameterized explosion model known as W7 (see, e.g., Nomoto et al. 1984), which can be approximated as a power law between velocity and density with an exponent of -7 (Branch et al. 1985). In order to account for deviations from the W7 power-law profile, we have left the power-law index as a free parameter in our study, the prior for which can be found in Table 1.

We approximate the elemental composition of the ejecta by assuming a uniform distribution of abundances above the photosphere (the same abundance values are used in each shell). We explored a set of abundances commonly used in the literature (e.g., Stehle et al. 2005; Sauer & Mazzali 2008; Kerzendorf 2011), namely carbon, magnesium, silicon, sulfur, calcium, titanium, and chromium. Iron, cobalt, and nickel abundances were split up into the decay chain of the isotope ⁵⁶Ni and stable iron. These elements account for the majority of the mass in explosion models and are well constrained by the spectra of SNe Ia (Filippenko 1997). The set of abundances (C, Mg, Si, S, Ca, Ti, Cr, Fe_{stable}, and ⁵⁶Ni) and explosion parameters (T_{inner} , v_{inner} , t_{exp} , and α_{ρ}) all together compose a 13-dimensional parameter space to model our spectra.

For the plasma state, we have chosen the nebular ionization approximation implemented in TARDIS and the dilute-lte excitation approximation. The radiation-matter interaction is modeled using the `macroatom` prescription. We have also set the number of packets to be equal to 400,000. The final spectral calculation uses the formal integral method (Lucy 1999) rather than straight packet statistics. The configuration of TARDIS can be found in Appendix B.

¹² The reference density is pre-computed from the power-law index to match that of the W7 model at 10000 km/s.

2.1. Model Evaluation

Spectral synthesis from our model with TARDIS, on average, takes approximately 10 minutes of CPU time on an Intel[®] Xeon[®] E5-2670 v2 CPU. Kerzendorf et al. (2021) estimated the time Required to explore a 20-parameter toy-model at this rate to be ~ 420 yr. Such a time constraint on model evaluation imposes a restriction upon our ability to use radiative transfer codes as a method of exploring the posterior distribution of SN Ia models. In order to subvert this restriction, we have implemented a technique for speeding up our model evaluation by eight orders of magnitude based upon the machine-learning framework developed by Kerzendorf et al. (2021). The estimation of our models through this technique is known as *emulation* and the machine-learning framework we used will from here on be referred to as the *emulator*. Details of the emulator including architecture, accuracy, and error analysis can be found in Appendix A. We find our emulator predicts the synthetic spectra produced by TARDIS given a set of model parameters within 1%, and therefore is an effective and necessary substitute for model evaluation.

3. Parameter Inference

Vectors of candidate input abundances (carbon, magnesium, etc.) and explosion parameters, $\vec{\theta} = \{C, Mg, \dots, t_{\text{exp}}, \alpha_p\}$, are drawn from a prior distribution described in Section 3.1. Model spectra are then produced by the emulator, where the emulated synthetic spectrum is predicted using the input parameters $\vec{\theta}$. We determine the likelihood of a given model through the application of a likelihood function described in Section 3.2. We have developed a non- χ^2 likelihood function that takes into account systematic differences between our theoretical and observed spectra. Lastly, in Section 3.3, we outline the Monte Carlo sampling technique used to construct the posterior distribution.

3.1. Prior Distribution

We developed a distribution from which to draw our prior samples based on parameters of SN Ia abundances taken from the Heidelberg Supernova Model Archive (HESMA). We specifically used the set of abundance profiles provided from various SNe Ia hydrodynamic simulations (Fink et al. 2014; Noebauer et al. 2017; Kromer et al. 2013, 2015; Sim et al. 2010; Noebauer et al. 2017; Fink et al. 2018; Marquardt et al. 2015; Fink et al. 2010b; Kromer et al. 2010; Sim et al. 2012; Gronow et al. 2020) to determine the range of input parameters. We determined the bounds of our prior by taking the 60% quantile of the distribution of abundances from the HESMA models where the shell velocity was above $10,000 \text{ km s}^{-1}$ in order to be consistent with the expected structure of the outer shells.

Abundances were sampled uniformly in log-space with any remaining abundance fraction filled in with oxygen such that all abundance fractions summed to unity. Oxygen is often used as a “filler” element in supernova fitting (e.g., Hachinger et al. 2017) due to the insensitivity to changes in the spectrum with respect to the oxygen mass fraction (see Hachinger 2011, Section 2.2.5.2). Therefore, the oxygen abundance is only determined implicitly and is not included as a model parameter.

For all other model parameters, we sampled along a uniform distribution. We used the values for explosion time, ejecta

velocity, photospheric boundary temperature, and density profile power-law exponent from the fit made by Kerzendorf (2011) as centroids. We then reviewed the works of Stehle et al. (2005) and Benetti et al. (2004) to determine reasonable ranges of uncertainties on these values, which were used to set the edges of the distribution. The range of values sampled for each parameter can be found in Table 1.

3.2. Likelihood Estimation

While our emulator accurately recreates the behavior of TARDIS under our spectral synthesis model, observations of real spectra are subject to physical and systematic biases. In order to compare our model spectra, $\hat{f}(\vec{\theta})$, to observation, f_{obs} , we develop a likelihood function, $\mathcal{L}(\vec{\theta})$, that corrects our model spectra and compares the results to our observed spectrum.

A correction function, $C(\hat{f}(\vec{\theta}))$, is applied to our model spectra. $C(\hat{f}(\vec{\theta}))$ first applies a redshift correction to set the frame of the model spectrum to the observed frame of SN 2002bo at $z=0.0042$ (Benetti et al. 2004). A host extinction correction is then performed using the model described by Cardelli et al. (1989) using $R_V=3.1$ (Schlafly & Finkbeiner 2011) and $E(B-V)=0.3$ (Benetti et al. 2004). Finally, a continuum removal technique described by Tonry & Davis (1979) and Blondin & Tonry (2007) is applied to the model spectrum. The continuum is estimated using a zero-mean 13-point cubic spline fit to the spectrum. We apply this continuum removal to our model spectra first, then we multiply by the continuum that would be removed by applying the same technique to the observed spectrum. Finally, the resulting continuum-removed model spectrum is linearly interpolated to the wavelength bins of the observed spectrum. Applying the corrections in this way allows us to compare our simulated spectra directly to the observed spectrum.

We compare our corrected model spectrum to the observed spectrum using a Gaussian likelihood function,

$$\log \mathcal{L}(\vec{\theta}) = -\frac{1}{2} \sum_{\lambda} \left[\frac{(C(\hat{f}(\vec{\theta})) - f_{\text{obs}})_{\lambda}^2}{s^2} + \log(2\pi s^2) \right],$$

where λ represents the wavelength bin of the observed spectrum of SN 2002bo in the observed frame. The parameter s^2 estimates the variance of our posterior distribution over model spectra, which we infer as another parameter (Hogg et al. 2010) with a log-uniform prior.

3.3. Posterior Distribution

The topology of the posterior distribution is unknown a priori, and could contain complicated degeneracies or multimodalities. Nested sampling (Skilling 2004; Buchner 2021a) is a robust Monte Carlo technique for this setting. We use the MLFriends algorithm (Buchner 2014, 2017) implemented in the *UltraNest* package (Buchner 2021b). The posterior distribution was explored with 400 live points. It converged to the target distribution after 10,000 iterations and required 1,000,000 model evaluations.

4. Results

Figure 1 shows the converged parameter distributions from our statistical inference. Silicon and sulfur abundances

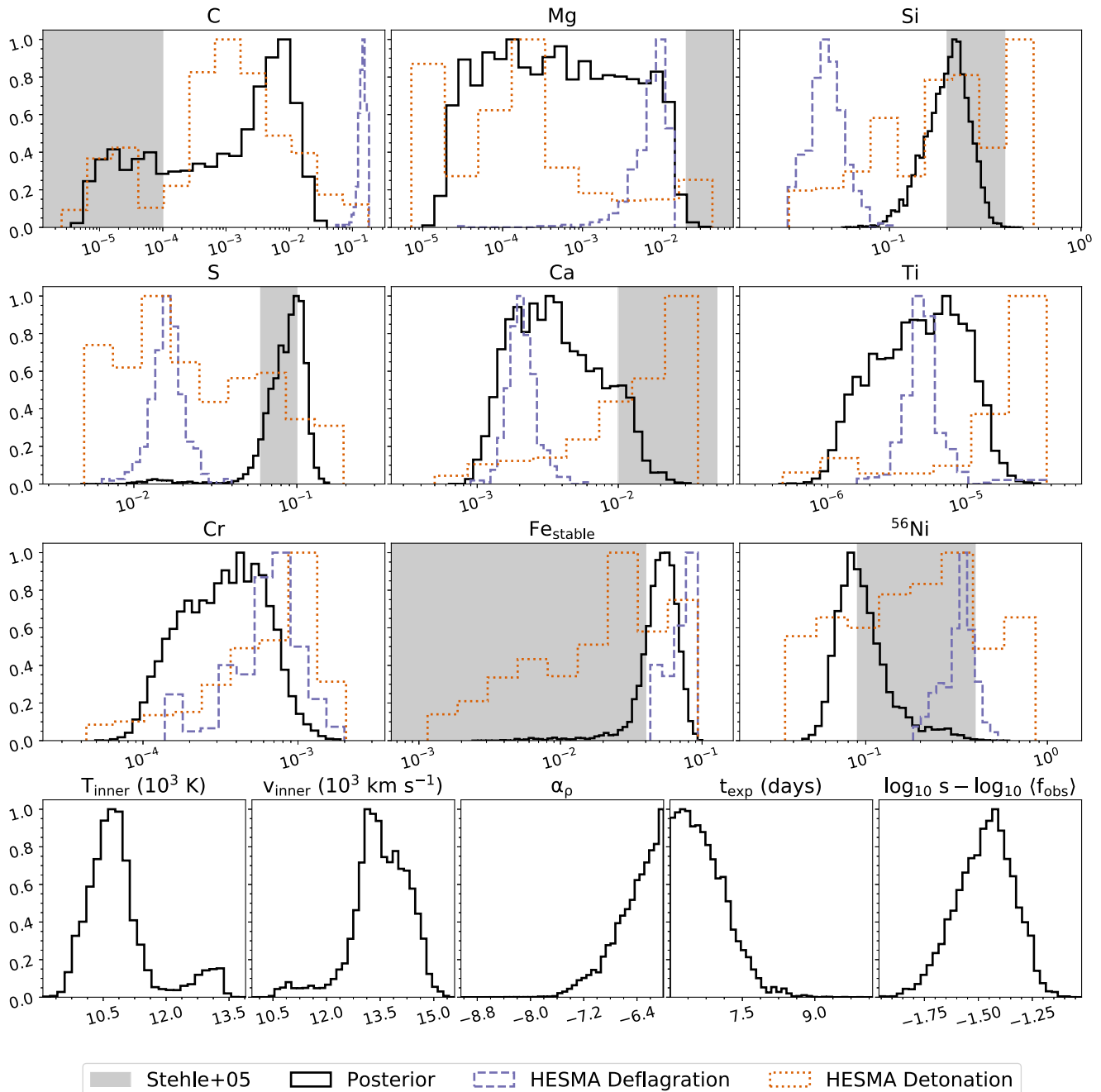


Figure 1. Posterior distribution of the parameter space sampled using nested sampling (black). Overlaid are distributions of elemental abundances above 10,000 km s⁻¹ taken from various HESMA models. Pure deflagration models are shown in purple while pure-detonation models are shown in orange. Deflagration to detonation transition (DDT) models are not included as they would not be noticeably distinguishable from pure-detonation models at this early epoch. Estimates of the range of abundances of elements in ejecta layers between 10,000 km s⁻¹ and 15,000 km s⁻¹ from Stehle et al. (2005) are represented by the gray shaded regions. Due to differences in methodology, we do not have reliable estimates for the abundances of titanium and chromium from Stehle et al. (2005).

contribute the largest fraction by mass of the ejecta, which can be inferred from the spectral features present in SN 2002bo. Stehle et al. (2005) used a similar code to TARDIS to manually fit the spectral time series of SN 2002bo. However, due to differences in methodologies, a direct comparison of elemental abundances is difficult and must be approximated. Because Stehle et al. (2005) does not provide uncertainties, we make the assumption that the uncertainty in their reported elemental abundances within various layers of the ejecta are comparable to those found in our study. Unfortunately, the full model inferred by Stehle et al. (2005) is not directly available for

download, so we estimate abundances in terms of mass fractions from the figures (Stehle et al. 2005, their Figure 5).

We compare our findings to their range of abundances reported in the velocity interval from 10,000 km s⁻¹ to 15,000 km s⁻¹ and generally find good agreement within our uncertainty ranges. We find a significant lack of carbon in the ejecta consistent with their analysis. The range of abundances determined from their analysis of silicon (0.2–0.4), sulfur (0.06–0.1), and ⁵⁶Ni (0.09–0.11) all overlap with our 68% confidence interval in Table 1. Their abundances of iron (<10⁻⁴–0.04) and calcium (0.01–0.05) were slightly outside

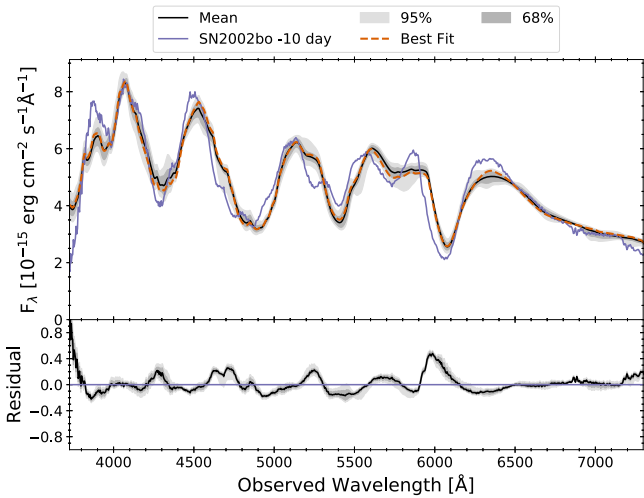


Figure 2. Fit to observed SN 2002bo –10 day spectrum (purple) using nested sampling to sample the posterior distribution. The best-fit spectrum (orange), represented by the maximum likelihood sample, shows a decent fit to the spectrum but misses features around 5972 Å and 3900 Å as well as much of the UV. The mean of the posterior distribution is shown in black with the 68% and 95% regions in gray and light gray, respectively. Posterior spectra are presented after application of the correction function described in Section 3.2. The residual distribution is shown as the fractional error between our posterior and our observed spectrum.

this region but are consistent if the level of uncertainty in their analysis is similar to ours. Individual values for both titanium and chromium are not available, so performing a direct comparison is not particularly reasonable or reliable.

By far our largest deviation from Stehle et al. (2005) is our magnesium abundance. Magnesium has the largest range of uncertainty in our analysis, spanning nearly four orders of magnitude. Operating under the assumption that the uncertainties in Stehle et al. (2005) are comparable to ours, not much information can be gathered from a comparison of values between the two studies as the magnesium abundance is mostly uninformative.

We constrain $t_{\text{exp}} = 6.64_{6.32}^{7.21}$ days,¹³ which is slightly below that of Benetti et al. (2004, $t_{\text{exp}} = 7.9 \pm 0.5$ days) and Stehle et al. (2005, $t_{\text{exp}} = 8.04$ days). Our estimates for both T_{inner} and v_{inner} are consistent with the range of values found by Stehle et al. (2005) for spectra between nearby epochs. The overall agreement of our results with similar previous attempts at manual fitting as well as theoretical models for SNe Ia explosion physics demonstrates that our model is consistent with the current literature.

There are a few notable mismatches between our posterior spectra and the observed spectrum (Figure 2). In the S II doublet our model over-fits the left peak and under-fits the right peak. This discrepancy is a common occurrence in radiative transfer model fits (see, e.g., Stehle et al. 2005) to SN Ia spectra and is due to a poor understanding of the lines lists and occupation numbers in this region. Since our abundance distribution through the ejecta is approximated to be uniform, the iron abundance in the outer layers is generally over-estimated. This causes line blanketing as the bluer packets are reflected back inward, resulting in a higher radiative temperature as well as less flux at the blue end of the spectrum. The higher temperatures affect the overall ionization state of the

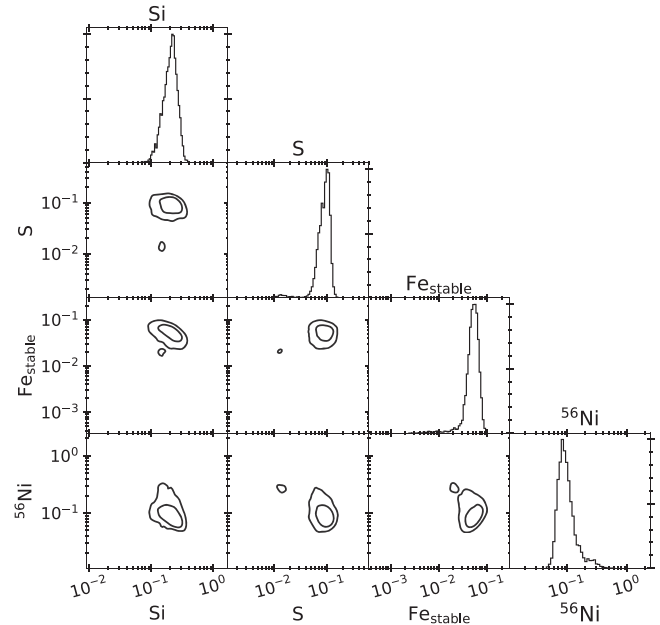


Figure 3. Posterior probability distribution of the elemental abundances of silicon, sulfur, stable iron, and ^{56}Ni . Contours show 68% and 95% confidence intervals of the Gaussian kernel density estimation (KDE) over the joint distribution of each parameter. Degeneracies and multimodalities in elemental abundances are apparent.

plasma causing the Si II to Si III ratio to decrease, weakening the Si II (5972 Å) feature. The poor fit to the Si II doublet is also seen in previous studies (see, e.g., Benetti et al. 2004).

We are able to perform a direct comparison of inferred model parameters of a real SN Ia spectrum to statistical samples of theoretical explosion models. In addition to the posterior distributions of the model parameters inferred for SN 2002bo, Figure 1 shows the distribution of abundances from two classes of models taken from the HESMA data sets above 10000 km/s corresponding to pure-deflagrations and pure-detonations. Deflagration to detonation transition (DDT) models are not included as they would be indistinguishable from pure-detonation models above the photosphere at these early times. The posterior distribution best matches with the distribution of abundances sampled from the HESMA detonation models, while mostly excluding the pure-deflagration models. The unfavorability of pure-deflagration models is strongly apparent for the distribution of carbon, sulfur, and silicon abundances in Figure 1. Calcium and chromium abundances slightly favor pure-deflagration hydrodynamic models, though their distribution widths are large and stretch over a few orders of magnitude, indicating that these abundances are not affecting the final shape of the spectrum significantly. We find that our initial modeling of the –10 day spectrum of SN 2002bo generally favors detonation or DDT models.

Figure 3 demonstrates the complexity of the posterior distribution of elemental abundances. A small multimodality in the sulfur abundance raises the possibility of manual fits becoming trapped in local minima. The joint probability distribution of stable iron with both silicon and ^{56}Ni is degenerate and multimodal. Such complexities indicate that any single set of model parameters may only describe one of a distribution of parameters that all appear to model the observed spectrum to similar accuracy. Despite some of the large variations and complexity in the posterior distribution of

¹³ See Table 1 for description of quantification.

parameters (Figure 1), the distribution of model spectra produced by these parameters (Figure 2) is within 3% variation of the mean of the observed spectrum.

5. Conclusion

We present a probabilistic reconstruction of a SN Ia explosion. Our results generally agree with manual fits (see, e.g., Stehle et al. 2005). We estimate the distribution of elemental abundances required to reproduce the observation of an early-time spectrum of SN 2002bo. Degeneracies and multimodalities in certain parameters showcase the need for a Bayesian treatment to draw secure physical conclusions, as similar spectra may be synthesized over a wide and complex space of parameters. The posterior distribution is compared to the distribution of elemental abundances computed from various explosion models in HESMA. We find that our analysis favors detonation models over pure-deflagration models. Given the speed and effectiveness of our modeling technique, we have demonstrated a new avenue for investigating the inner mechanisms driving SN Ia explosions.

6. Contributor Roles

1. Conceptualization: John O'Brien, Wolfgang Kerzendorf
2. Data curation: John O'Brien
3. Formal analysis: John O'Brien, Wolfgang Kerzendorf
4. Funding acquisition: Wolfgang Kerzendorf
5. Investigation: John O'Brien
6. Methodology: John O'Brien, Wolfgang Kerzendorf
7. Project administration: Wolfgang Kerzendorf
8. Resources: Institute for Cyber-Enabled Research at Michigan State University
9. Software: John O'Brien, Wolfgang Kerzendorf, Marc Williamson, Johannes Buchner, Christian Vogl, James Gillanders, TARDIS Collaboration
10. Supervision: Wolfgang Kerzendorf
11. Validation: John O'Brien
12. Visualization: John O'Brien, James Gillanders
13. Writing original draft: John O'Brien, Wolfgang Kerzendorf
14. Writing, review, and editing: John O'Brien, Andrew Fullard, Marc Williamson, Patrick van der Smagt, Johannes Buchner, James Gillanders, Wolfgang Kerzendorf, Rüdiger Pakmor, Andreas Flörs, Stephan Hachinger, Christian Vogl, Stuart Sim, Maryam Modjaz

We would like to thank Stuart Sim and Maryam Modjaz for their edits and suggestions.

This work was supported in part through computational resources and services provided by the Institute for Cyber-Enabled Research at Michigan State University.

This work made use of the Heidelberg Supernova Model Archive (HESMA), <https://hesma.h-its.org>

This research made use of TARDIS, a community-developed software package for spectral synthesis in supernovae (Kerzendorf & Sim 2014; Kerzendorf et al. 2021). The development of TARDIS received support from the Google Summer of Code initiative, from ESA's Summer of Code in Space program, and from NumFOCUS's Small Development Grant. TARDIS makes extensive use of Astropy and PyNE.

This work would not have been possible without the large open source software community providing powerful numerical, scientific, visualization, machine-learning, and astrophysical

libraries: Astropy¹⁴ (Astropy Collaboration et al. 2013, 2018), extinction¹⁵ (Barbary 2016), Matplotlib¹⁶ (Hunter 2007), Numba¹⁷ (Lam et al. 2015), NumPy¹⁸ (Harris et al. 2020), pandas¹⁹ (McKinney 2010), scikit-learn²⁰ (Pedregosa et al. 2011), SciPy²¹ (Virtanen et al. 2020), TensorFlow²² (Abadi et al. 2015), and UltraNest²³ (Buchner 2014, 2019). We would like to thank these communities for providing and maintaining the resources that allow science to be done in an open, replicable, and accessible way.

C.V. was supported for this work by the Excellence Cluster ORIGINS, which is funded by the Deutsche Forschungsgemeinschaft (DFG, German Research Foundation) under Germany's Excellence Strategy-EXC-2094-390783311.

Appendix A Emulator

Emulation is the practice of developing some analytic function that approximates the behavior of another function. TARDIS can be thought of as a function mapping a vector of supernova parameters to a vector representing a spectrum. We extend the techniques described in the Kerzendorf et al. (2021) paper to make an emulator for the -10 day spectrum of SN 2002bo. The method proposed by Kerzendorf et al. (2020) uses an ensemble of feed-forward neural networks to emulate the spectrum computation. Our neural network is trained from a set of pre-computed data points, composed of training spectra over a grid spanning a physically plausible parameter space for a SN Ia. The goal for the emulator is to be used in our parameter inference so we ensure that the training set parameter space contains the final prior fitting space (see Section 3.1).

We changed several parts of the procedure when compared to the emulator described by Kerzendorf et al. (2021). One key difference is the addition of two parameters: the power-law index α_p and the time since explosion t_{exp} . The bounds on parameters corresponding to computed spectra were also modified to encompass elemental abundances corresponding to shells above 8000 km s^{-1} in HESMA models. Kerzendorf et al. (2021) presented an ensemble of different neural network architectures that could reproduce simulated TARDIS spectra to a high degree of precision. For computational efficiency, for this Letter we chose only a single network from the neural networks described by Kerzendorf et al. (2021). Specifically, we used a model which propagates the 14 inputs through three subsequent hidden layers of 400 neurons each, reaching 500 outputs. The hidden units used the "softplus" activation function. We trained our emulator with the "nadam" optimizer on a 91000 sample training set and 39000 sample validation set in a 70%/30% training/validation split. Training time was 20 minutes on an NVIDIA® GeForce® RTX 2080Ti GPU.

The measured accuracy of our emulator using the mean and maximum fractional error (Figure A1) is similar to that of the

¹⁴ <https://www.astropy.org>

¹⁵ <https://extinction.readthedocs.io/en/latest>

¹⁶ <https://matplotlib.org>

¹⁷ <https://numba.pydata.org>

¹⁸ <https://numpy.org>

¹⁹ <https://pandas.pydata.org>

²⁰ <https://scikit-learn.org>

²¹ <https://www.scipy.org/>

²² <https://www.tensorflow.org/>

²³ <https://johannesbuchner.github.io/UltraNest>

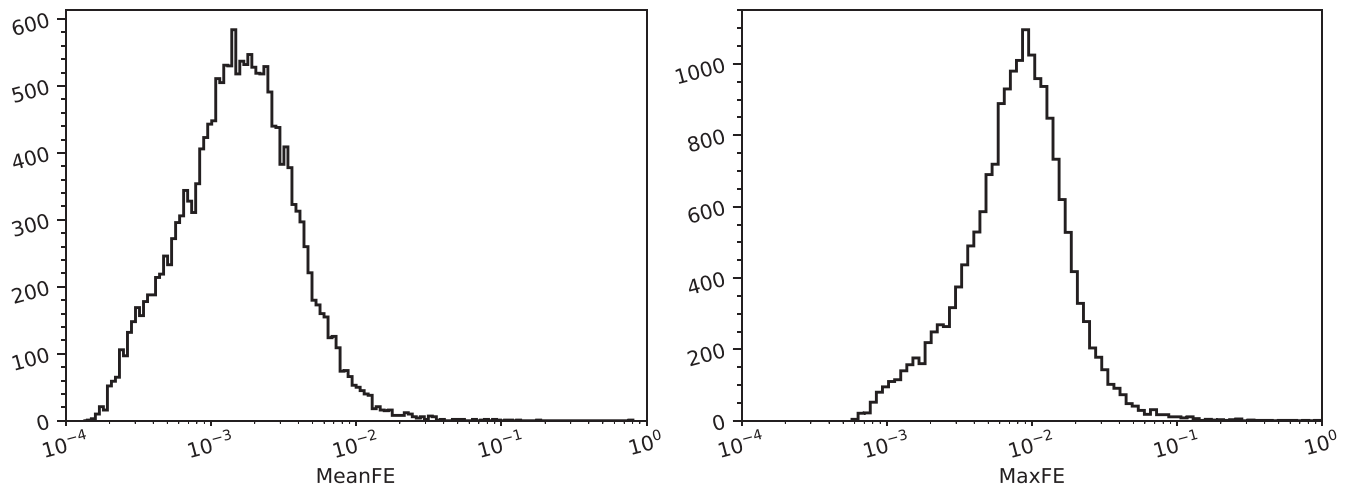


Figure A1. Mean and maximum fractional error for our TARDIS emulator. Test spectra are compared to emulated spectra generated using the same parameter set. The low level of error demonstrates that our emulator is effective at modeling the physics of TARDIS. Descriptions of the mean and maximum fractional error can be found in Kerzendorf et al. (2021).

initial DALEK emulator. Figure A1 shows that our mean fractional error is almost always below 1% over our validation set. The final fit presented in Section 4 has a mean fractional error of 10% between the observed spectrum and the maximum posterior model indicating that any uncertainty from our emulation is less than systematics for the presented work.

Appendix B External Links to Data

The TARDIS configuration file, posterior samples with their associated weights, and the parameter grid and corresponding spectra used in training the emulator are provided through Zenodo:[10.5281/zenodo.5007378](https://zenodo.org/record/5007378). The observed spectrum of SN 2002bo used in this Letter is hosted by the [Open Supernova Catalog](#) (Guillochon et al. 2017).

ORCID iDs

John T. O'Brien [ORCID](https://orcid.org/0000-0003-3615-9593) <https://orcid.org/0000-0003-3615-9593>
 Wolfgang E. Kerzendorf [ORCID](https://orcid.org/0000-0002-0479-7235) <https://orcid.org/0000-0002-0479-7235>
 Marc Williamson [ORCID](https://orcid.org/0000-0003-2544-4516) <https://orcid.org/0000-0003-2544-4516>
 Rüdiger Pakmor [ORCID](https://orcid.org/0000-0003-3308-2420) <https://orcid.org/0000-0003-3308-2420>
 Johannes Buchner [ORCID](https://orcid.org/0000-0003-0426-6634) <https://orcid.org/0000-0003-0426-6634>
 James H. Gillanders [ORCID](https://orcid.org/0000-0002-8094-6108) <https://orcid.org/0000-0002-8094-6108>
 Patrick van der Smagt [ORCID](https://orcid.org/0000-0003-4418-4916) <https://orcid.org/0000-0003-4418-4916>

References

- Abadi, M., Agarwal, A., Barham, P., et al. 2015, TensorFlow: Large-Scale Machine Learning on Heterogeneous Systems, <http://tensorflow.org/>
 Astropy Collaboration, Price-Whelan, A. M., Sipőcz, B. M., et al. 2018, *AJ*, **156**, 123
 Astropy Collaboration, Robitaille, T. P., Tollerud, E. J., et al. 2013, *A&A*, **558**, A33
 Barbary, K. 2016, Extinction v0.3.0, Zenodo, doi:[10.5281/zenodo.804967](https://zenodo.org/record/804967)
 Barna, B., Szalai, T., Kromer, M., et al. 2017, *MNRAS*, **471**, 4865
 Benetti, S., Meikle, P., Stehle, M., et al. 2004, *MNRAS*, **348**, 261
 Blondin, S., Matheson, T., Kirshner, R. P., et al. 2012, *AJ*, **143**, 126
 Blondin, S., & Tonry, J. L. 2007, *ApJ*, **666**, 1024
 Boyle, A., Sim, S. A., Hachinger, S., & Kerzendorf, W. 2017, *A&A*, **599**, A46
 Branch, D. 1992, *ApJ*, **392**, 35
 Branch, D., Dang, L. C., Hall, N., et al. 2006, *PASP*, **118**, 560
 Branch, D., Doggett, J. B., Nomoto, K., & Thielemann, F. K. 1985, *ApJ*, **294**, 619
 Branch, D., Fisher, A., & Nugent, P. 1993, *AJ*, **106**, 2383
 Buchner, J. 2014, *Statistics and Computing*, **26**, 383
 Buchner, J. 2017, arXiv:[1707.04476](https://arxiv.org/abs/1707.04476)
 Buchner, J. 2019, *PASP*, **131**, 108005
 Buchner, J. 2021a, arXiv:[2101.09675](https://arxiv.org/abs/2101.09675)
 Buchner, J. 2021b, *JOSS*, **6**, 3001
 Cardelli, J. A., Clayton, G. C., & Mathis, J. S. 1989, *ApJ*, **345**, 245
 Colgate, S. A., & McKee, C. 1969, *ApJ*, **157**, 623
 Filippenko, A. V. 1997, *ARA&A*, **35**, 309
 Fink, M., Kromer, M., Hillebrandt, W., et al. 2018, *A&A*, **618**, A124
 Fink, M., Kromer, M., Seitenzahl, I. R., et al. 2014, *MNRAS*, **438**, 1762
 Fink, M., Röpke, F. K., Hillebrandt, W., et al. 2010a, *A&A*, **514**, A53
 Fink, M., Röpke, F. K., Hillebrandt, W., et al. 2010b, *A&A*, **514**, A53
 Gillanders, J. H., Sim, S. A., & Smartt, S. J. 2020, *MNRAS*, **497**, 246
 Gronow, S., Collins, C., Ohlmann, S. T., et al. 2020, *A&A*, **635**, A169
 Guillochon, J., Parrent, J., Kelley, L. Z., & Margutti, R. 2017, *ApJ*, **835**, 64
 Hachinger, S. 2011, PhD thesis, TU München
 Hachinger, S., Röpke, F. K., Mazzali, P. A., et al. 2017, *MNRAS*, **471**, 491
 Harris, C. R., Millman, K. J., van der Walt, S. J., et al. 2020, *Natur*, **585**, 357
 Hogg, D. W., Bovy, J., & Lang, D. 2010, arXiv:[1008.4686](https://arxiv.org/abs/1008.4686)
 Hunter, J. D. 2007, *CSE*, **9**, 90
 Iben, I. J., & Tutukov, A. V. 1984, *ApJS*, **54**, 335
 Kashi, A., & Soker, N. 2011, *MNRAS*, **417**, 1466
 Kerzendorf, W., Sim, S., Vogl, C., et al. 2021, tardis-sn/tardis: TARDIS v3.0. dev4010, v3.0.dev4010, Zenodo, doi:[10.5281/zenodo.4995779](https://zenodo.org/record/4995779)
 Kerzendorf, W. E. 2011, PhD thesis, Australian National University, Research School of Astronomy Astrophysics
 Kerzendorf, W. E., & Sim, S. A. 2014, *MNRAS*, **440**, 387
 Kerzendorf, W. E., Vogl, C., Buchner, J., et al. 2021, *ApJL*, **910**, L23
 Kobayashi, C., Karakas, A. I., & Lugaro, M. 2020, *ApJ*, **900**, 179
 Kromer, M., Fink, M., Stanishev, V., et al. 2013, *MNRAS*, **429**, 2287
 Kromer, M., Ohlmann, S. T., Pakmor, R., et al. 2015, *MNRAS*, **450**, 3045
 Kromer, M., Sim, S. A., Fink, M., et al. 2010, *ApJ*, **719**, 1067
 Lam, S. K., Pitrou, A., & Seibert, S. 2015, in Proc. Second Workshop on the LLVM Compiler Infrastructure in HPC, ed. H. Finkel (New York: ACM), 1
 Livio, M., & Riess, A. G. 2003, *ApJ*, **594**, L93
 Lucy, L. B. 1999, *A&A*, **345**, 211
 Magee, M. R., Kotak, R., Sim, S. A., et al. 2016, *A&A*, **589**, A89
 Marquardt, K. S., Sim, S. A., Ruiters, A. J., et al. 2015, *A&A*, **580**, A118
 Mazzali, P. A., Röpke, F. K., Benetti, S., & Hillebrandt, W. 2007, *Sci*, **315**, 825
 McKinney, W. 2010, in Proc. 9th Python in Science Conf., SciPy 2010, ed. S. van der Walt & J. Millman, 56
 Noebauer, U. M., Kromer, M., Taubenberger, S., et al. 2017, *MNRAS*, **472**, 2787
 Nomoto, K. 1982, *ApJ*, **257**, 780
 Nomoto, K., Thielemann, F. K., & Yokoi, K. 1984, *ApJ*, **286**, 644
 Pedregosa, F., Varoquaux, G., Gramfort, A., et al. 2011, *JMLR*, **12**, 2825
 Phillips, M. M. 1993, *ApJL*, **413**, L105

- Polin, A., Nugent, P., & Kasen, D. 2019, *ApJ*, **873**, 84
- Riess, A. G., Filippenko, A. V., Challis, P., et al. 1998, *AJ*, **116**, 1009
- Sauer, D., & Mazzali, P. 2008, *NewAR*, **52**, 370
- Schlafly, E. F., & Finkbeiner, D. P. 2011, *ApJ*, **737**, 103
- Shen, K. J., Kasen, D., Miles, B. J., & Townsley, D. M. 2018, *ApJ*, **854**, 52
- Sim, S. A., Fink, M., Kromer, M., et al. 2012, *MNRAS*, **420**, 3003
- Sim, S. A., Röpke, F. K., Hillebrandt, W., et al. 2010, *ApJL*, **714**, L52
- Skilling, J. 2004, in *AIP Conf. Ser.*, 735, *Bayesian Inference and Maximum Entropy Methods in Science and Engineering*, ed. R. Fischer, R. Preuss, & U. V. Toussaint (Melville, NY: AIP), 395
- Stehle, M., Mazzali, P. A., Benetti, S., & Hillebrandt, W. 2005, *MNRAS*, **360**, 1231
- Tonry, J., & Davis, M. 1979, *AJ*, **84**, 1511
- van Kerkwijk, M. H., Chang, P., & Justham, S. 2010, *ApJ*, **722**, L157
- Virtanen, P., Gommers, R., Oliphant, T. E., et al. 2020, *NatMe*, **17**, 261
- Vogl, C., Kerzendorf, W. E., Sim, S. A., et al. 2020, *A&A*, **633**, A88
- Webbink, R. F. 1984, *ApJ*, **277**, 355
- Whelan, J., & Iben, I. J. 1973, *ApJ*, **186**, 1007
- Williamson, M., Kerzendorf, W., & Modjaz, M. 2021, *ApJ*, **908**, 150
- Woosley, S. E., & Weaver, T. A. 1994, *ApJ*, **423**, 371